Superlattices and Microstructures 77 (2015) 305–312

Contents lists available at ScienceDirect

Superlattices and Microstructures

journal homepage: www.elsevier.com/locate/superlattices

Solution-based synthesis of high yield CZTS (Cu_2ZnSnS_4) spherical quantum dots

G. Rajesh [a,*], N. Muthukumarasamy [a], E.P. Subramanian [b], M.R. Venkatraman [a], S. Agilan [a], V. Ragavendran [c], M. Thambidurai [d], S. Velumani [e], Junsin Yi [f], Dhayalan Velauthapillai [g]

[a] Dept of Physics, Coimbatore Institute of Technology, Coimbatore, India
[b] Dept of Chemistry, Coimbatore Institute of Technology, Coimbatore, India
[c] Dept of Material Science, School of Chemistry, Madurai Kamaraj University, Madurai, India
[d] Dept of Electrical and Computer Engineering, Global Frontier Center for Multiscale Energy Systems, Seoul National University, Seoul, South Korea
[e] Department of Electrical Engineering (SEES), Ave IPN 2508, CINVESTAV, Zacatenco, Mexico City CP 06730, Mexico
[f] College of Information and Communication Engineering, Sungkyunkwan University, Suwon 440-746, Republic of Korea
[g] Dept of Engineering, University College of Bergen, Bergen, Norway

ARTICLE INFO

Article history:
Received 12 November 2014
Accepted 15 November 2014
Available online 25 November 2014

Keywords:
Chemical precipitation technique
Quantum dots
High yield
Low temperature

ABSTRACT

High yield CZTS quantum dots have been synthesized using simple precursors by chemical precipitation technique. Formation mechanism of CZTS spherical quantum dots also has been investigated. According to the mechanism, copper sulfide nuclei firstly forms, and serves as the starting point for the nucleation and growth of CZTS. X-ray diffraction pattern, X-ray photoelectron spectra (XPS) and Raman spectra reveals the formation of pure kesterite structure Cu_2ZnSnS_4 nanoparticles. HRTEM analysis reveals the formation of CZTS quantum dots with an average particle size of ~8.3 nm. The elemental distribution of CZTS quantum dots studied using STEM elemental mapping reveals that Cu, Zn, Sn and S are present in the sample. The photoluminescence spectra of CZTS exhibit a broad red emission band at 657 nm. The optical band gap is shifted to the higher energy side and it shows the presence of quantum confinement effect.

* Corresponding author. Tel.: +91 9790380428.
E-mail address: rajesh.govind88@gmail.com (G. Rajesh).

http://dx.doi.org/10.1016/j.spmi.2014.11.016
0749-6036/

Nanomaterials exhibit electrical and optical properties which depend sensitively on the size of the nanocrystals and the properties are of both fundamental and technological interest. Among various types of chalcogenide materials, $CuInSe_2$ (CIS), $CuInGa(S,Se)_2$(CIGS) and CdTe are the most prominent and commercialized materials for large scale photovoltaic manufacturing due to their high power conversion efficiency and stability [1]. However, the low availability and toxicity of indium and gallium increases the production costs and hinders the development of CIGS thin film solar cells [2]. The toxicity of heavy metal cadmium in CdTe based solar cells also raises health and environmental concerns. The crystal structure of CZTS is similar to that of (CIGS) $CuIn_{1-x}Ga_xSe_2$ which is considered as the most promising solar cell absorber layer. However, the constituent elements In and Ga are expensive and Se is toxic. In contrast to CIGS, CZTS has attracted much attention in recent years because of its abundant availability and non-toxic nature [3]. In order to replace rare or toxic elements in a compound semiconductor, isoelectronic alteration can be made to obtain a new compound semiconductor with the same electronic structure. In CIGS compound semiconductor indium and gallium can be replaced by Zn and Sn, as they are non-toxic and abundantly available materials and replacing Se with S converts CIGS into CZTS. Kesterite, Cu_2ZnSnS_4 (CZTS), $Cu_2ZnSnSe_4$ (CZTSe) and their alloys ($Cu_2ZnSn(S,Se)_4$ (CZTSSe)), are regarded as promising absorber materials for future photovoltaic systems on a terra-watt scale [4–6].

On the other hand, tremendous amount of interest has been shown in semiconductor nanoparticles for the fabrication of highly efficient quantum dot solar cells because the nanoparticles exhibit size – dependent energy structure and unique carrier generation, such as hot carrier extraction and multiexciton generation derived from quantum size effect [7–11]. The theoretical solar energy conversion efficiency of quantum dot solar cells has been reported to be ca. 60% [9] which is much higher than Shockley–Quisser limit (32%) [12].

CZTS nano particles can be synthesized by various methods such as, solvothermal [13], hot injection [14], hydrazine slurry-based methods [15], microwave assisted methods [16] and sol–gel [17]. The wet chemical synthesis of CZTS nanoparticles offers unique tools to carefully control the particle size, phase composition and surface properties at nano scale level. So far, very few investigations have been reported on CZTS quantum dots [18,25] and also low temperature, high yield synthesis of CZTS nano particles has been limited. In this letter we report about the quantitative yield of CZTS quantum dots prepared using simple precursors at low temperature by chemical precipitation technique. To synthesize high yield, single phase kesterite CZTS the precursor materials of CZTS are dissolved in long chain coordinating solvents followed by burst precipitation and controlled growth at desired temperature [19]. Analytical reagent grade (AR) chemicals copper nitrate ($Cu(NO_3)_2$) (0.20 M), zinc nitrate ($Zn(NO_3)_2$) (0.15 M), tin chloride ($SnCl_4$) (0.15 M), and thiourea (H_2NCSNH_2) (0.40 M) were dissolved in 2-methoxy ethanol and ethanolamine was added dropwise at room temperature. The resultant solution was stirred for 1 h to yield a homogeneous, clear and transparent solution using magnetic stirrer. The obtained solution was aged at room temperature for 48 h for the nucleation and growth of CZTS nanoparticles. The obtained precipitate was washed several times with distilled water and centrifuged at 5000 rpm for 10 min, further it was dried at 70 °C for 1 h. The synthesized nanoparticles were annealed at 170 °C for 1 h. The reaction mechanism of CZTS has been reported in our earlier work [27].

Structural properties of CZTS nanoparticles were studied using X-ray diffractometer Bruker D8 and Raman spectroscopy studies were carried out using Raman spectrometer (Horiba-Jobin Labram 800 HR). High-resolution TEM (HRTEM) and selected area diffraction pattern images were recorded using HRTEM (JEOL, JEM-ARM200F). The elemental distribution of CZTS nanoparticles was studied using STEM instrument attached to the HRTEM. The photoluminescence spectra were recorded using (Lab-RAM HR800). X-ray photoelectron Spectroscopy (XPS) studies were carried out using ESCA2000 (VG microtech: UK). Optical properties were studied using the absorbance spectra recorded using UV–Vis–NIR spectrophotometer (Jasco V570).

TEM image of the CZTS nanoparticles is shown in Fig. 1(a) and it is observed that all the particles are spherical in shape. Fig. 1(b and c) shows the high-resolution transmission electron microscopy (HRTEM) image of CZTS nano particles. The image clearly shows the lattice fringes indicating the formation of good nano crystalline CZTS quantum dots. The HRTEM image gives a grain size of ~8.3 nm. This confirms the formation of CZTS nano particles with particle size lying in the quantum

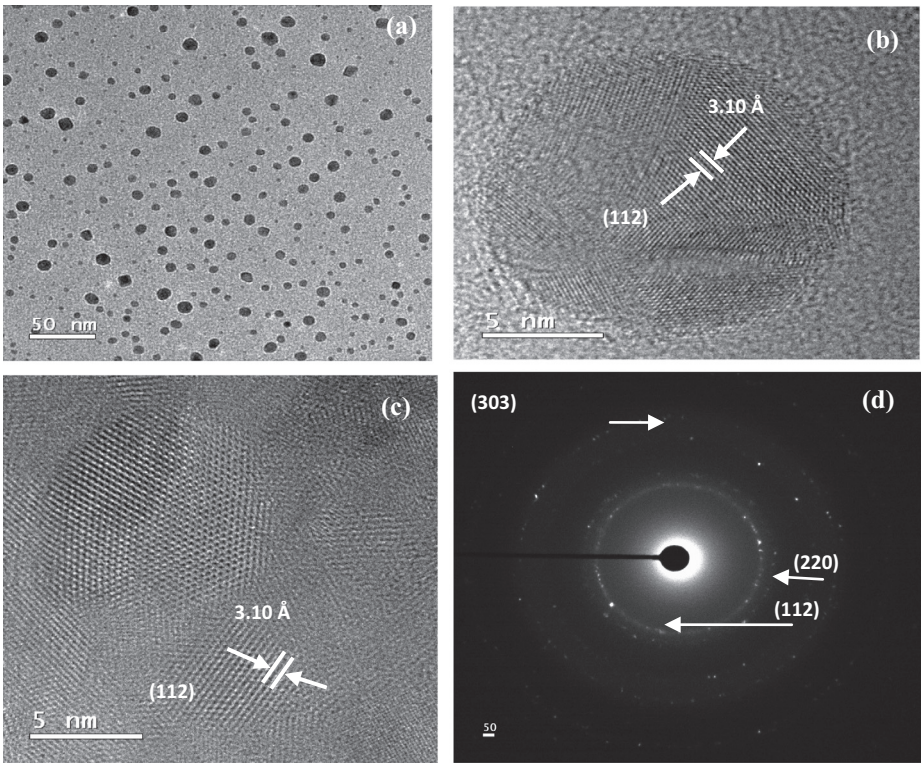

Fig. 1. (a) TEM image of CZTS nanoparticles, (b and c) HRTEM image of CZTS quantum dots, (d) SAED pattern of CZTS quantum dots.

dot range. The HRTEM image exhibits lattice fringes with *d* spacing of 3.10 Å corresponding to the (1 1 2) reflection of the kesterite phase CZTS. Selected area electron diffraction (SAED) image shown in Fig. 1(c) exhibits diffraction rings corresponding to the (1 1 2), (2 2 0), and (3 0 3) directions of the kesterite phase of CZTS. The d spacing values obtained for all the diffraction rings from the SAED pattern match very well with that of kesterite CZTS. The appearance of multiple diffraction rings is due to the random orientation of the polycrystallites. The spotty ring pattern with missing periodicity observed in the SAED image is due to the fact that the particles have random orientation.

Fig. 2 shows the X-ray diffraction pattern of the CZTS quantum dots. The diffraction pattern exhibits broad peaks revealing that the synthesized particles have very small crystallite size. The peaks obtained at the 2θ positions 28.26, 47.28, 55.24 corresponds to the (1 1 2), (2 2 0), (3 1 2) planes of CZTS nanoparticles and they are characteristic of tetragonal type kesterite structure of Cu_2ZnSnS_4 (JCPDS, card No. 26-0575) [20]. Kesterite has a tetragonal unit cell inside which each sulfur anion is bonded to four cations and each cation is bonded to four sulfur anions. The cation layers alternate with sulfur anion layers along the crystallographic *c*-direction as CuZn/SS/CuSn/SS [28].

The average crystallite size of the CZTS nanoparticle was calculated and found to be ~9.1 nm by using Scherer's equation. Being quaternary compound CZTS often contains other binary and ternary phases and it is difficult to control the stoichiometry. Most of the secondary phases such as (ZnS, CuS, Sn_2S_3, SnS_2 and Cu_2SnS_3) are formed due to the lack of sulfur during the formation of CZTS. The secondary phases have peaks which lie close to the peaks of CZTS due to similar crystal structure and this makes it hard to distinguish CZTS from the secondary phase in a X-ray diffractogram. Most of the reports shows that CZTS loses its anion during annealing process due to the high volatile nature of sulfur. Therefore, CZTS annealed without sulfur atmosphere exhibits secondary phases [21]. Raman

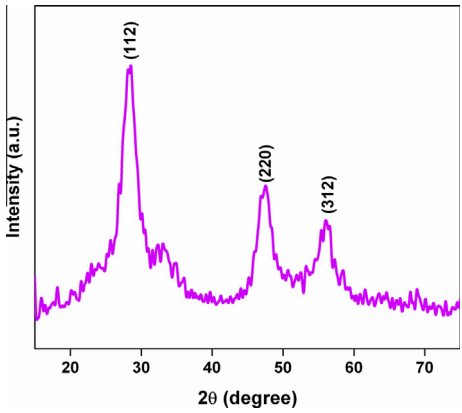

Fig. 2. X-ray diffraction pattern of CZTS quantum dots.

spectroscopy can give a better indication of the presence of secondary phase, because each phase in CZTS will give a peak position in Raman scattering which is more distinct than in X-ray diffraction pattern.

The Raman spectra of CZTS film is shown in Fig. 3. The vibration frequency at 332 cm^{-1} confirms the formation of pure kesterite phase CZTS. The strong peak observed at 332 cm^{-1} corresponds to the A1 mode of CZTS. The A1 modes are pure anion modes which correspond to vibrations of Sulfur atoms surrounded by motionless neighboring atoms [29] and their broadening suggests the phonon confinement effect occurring in the nanoparticles. A relationship between nano-crystal size and phonon position can be expressed (based on uncertainty principle)

$$\Delta P \Delta X \geq \hbar^2/4$$

where ΔP is phonon momentum distribution, ΔX is particle size distribution, and ħ is reduced Planck's constant. The reduction in particle size will result in confinement of phonon within the particle. The CZTS Raman spectrum did not show any evidence for the presence of binary phases SnS, SnS_2, CuS and Cu_2S.

Fig. 4(a and b) shows the high resolution STEM image of CZTS Quantum dots. In order to identify the elemental distribution of the CZTS nanoparticle, chemical analysis with nanoscale spatial resolution was carried out using STEM elemental mapping shown in Fig. 4(c–f). The images show the homogeneous and uniform distribution of all the four elements Cu, Zn, Sn&S.

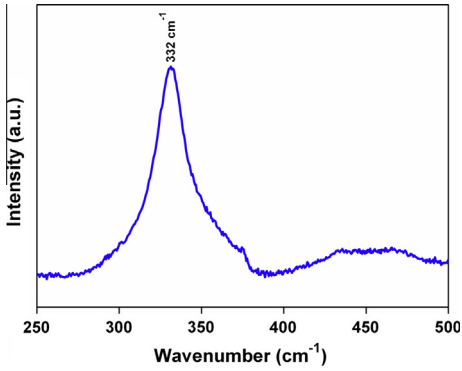

Fig. 3. Raman spectrum of kesterite phase CZTS quantum dots.

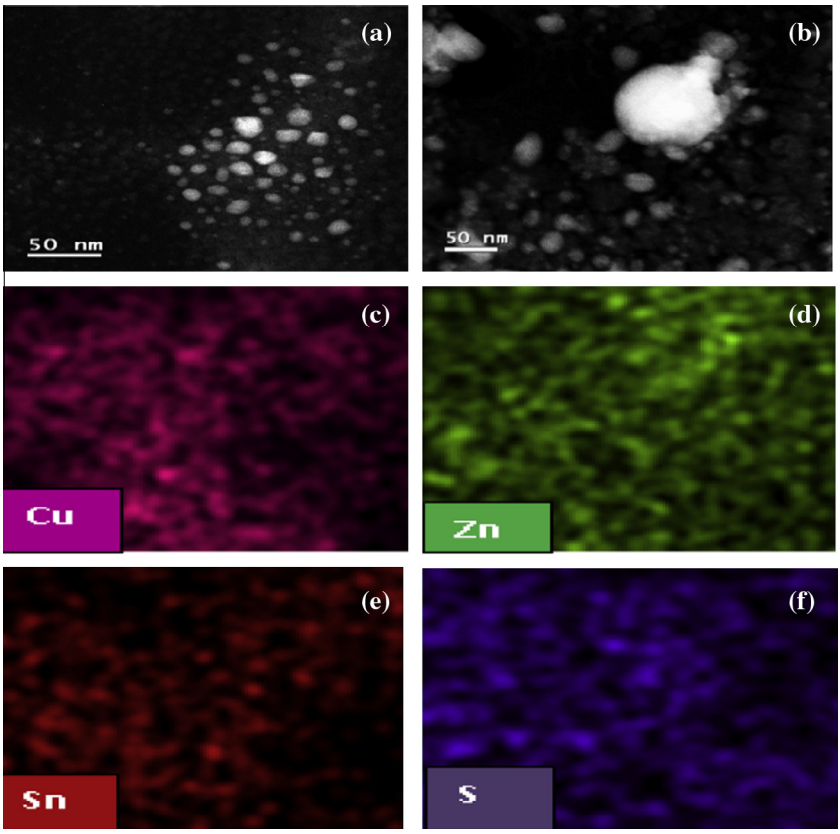

Fig. 4. ((a) and (b)) Scanning transmission electron micrographs of kesterite CZTS quantum dots. (c–f) STEM elemental mapping images of CZTS quantum dots.

X-ray photoelectron spectroscopy (XPS) was carried out to investigate the stoichiometry and the oxidation states of constituent elements in the CZTS nano particles. The core level spectra of Cu 2p, Zn 2p, Sn 3d and S 2p are shown in Fig. 5. The peak of Cu 2p split into 931.4 eV (2p3/2) and 951.3 eV (2p1/2) with a splitting energy of 19.9 eV is assigned to Cu(I). The 2p peak of Zn observed at the binding energies of 1021.5 (2p3/2) and 1044.3 eV (2p1/2) with a splitting energy of 22.8 eV correspond to Zn(II). The peak of Sn 3d split into 486.2 (2p5/2) and 494.6 eV (2p3/2) with a splitting energy of 8.4 eV is attributed to Sn(IV). The 2p peak of S lying in the range of 160–164 eV suggests its sulfide states [26].

The formation of CZTS nanoparticles can be also confirmed by photoluminescence (PL) spectroscopy. Fig. 6 shows the PL spectra of CZTS nanoparticles recorded at room temperature using an excitation wavelength of 620 nm. The spectra is found to exhibit two emission peaks centered on 657 and 691 nm. The strong emission band is observed at 657 nm and weak band cover the region between 675 and 710 nm. The observed emission bands are in red region (620–740 nm) of the electromagnetic spectrum. Emissions from semiconductor nanoparticles originate from electrons in the conduction band, excitonic states and trap states. It is important to note that any physical property that is dependent on the size of a quantum dot could also be used for predicting its size and distribution. It is well known that emission is very sensitive to nature of nanoparticle surface because of the presence of gap surface states arising from surface non stoichiometry and unsaturated bonds.

The absorbance spectra of the kesterite CZTS quantum dots is shown in Fig. 7. The inset in the figure shows the $(\alpha h\upsilon)^2$ versus $(h\upsilon)$ plot of the CZTS quantum dots. The valence band is made by an

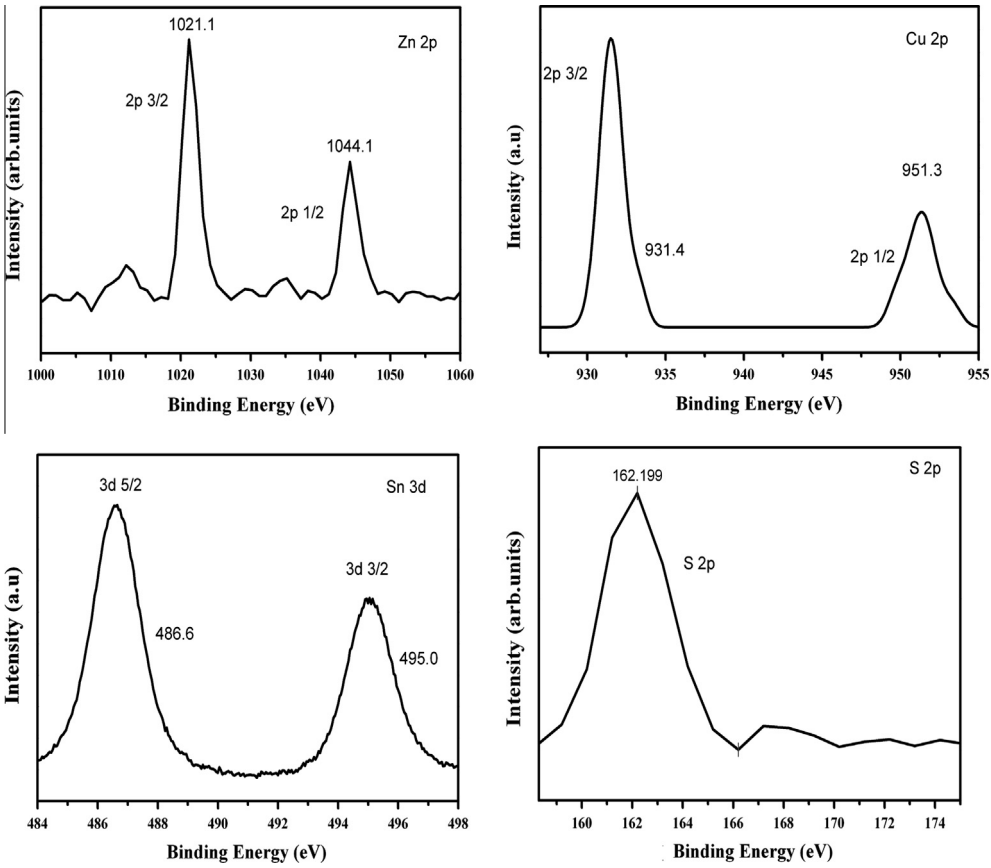

Fig. 5. XPS Spectra of CZTS quantum dots.

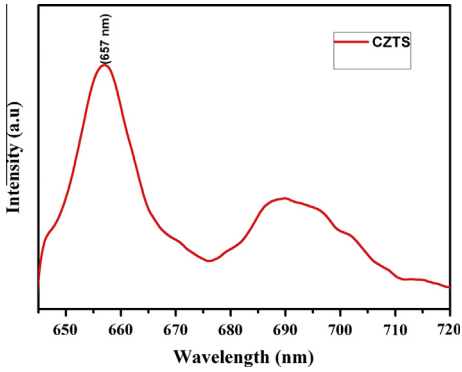

Fig. 6. Photoluminescence spectra of CZTS quantum dots.

antibonding linear combination of Cu-3d states and S-3p states, and the conduction band is dominated by an isolated band made up by Sn-5s and S-3p states. The transitions from the Cu-3d/S-3p states into the conduction band determine the optical properties of CZTS in the visible wavelength [33,34].

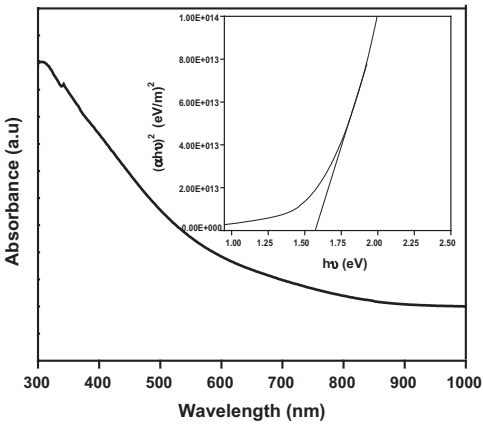

Fig. 7. Absorption spectra of CZTS nanoparticles inset plot of $(\alpha h\upsilon)^2$ versus $(h\upsilon)$.

The band gap of the CZTS quantum dots has been determined using the relation,

$$\alpha = A(h\upsilon - E_g)^{1/2}$$

where α is the absorption coefficient, A is the constant, E_g is the energy gap and $h\upsilon$' is the incident photon energy.

The optical band gap is deduced by extrapolating the straight line portion of the $(\alpha h\upsilon)^2$ versus $(h\upsilon)$ plot to meet the $h\upsilon$ axis. The optical band gap energy was found to be 1.58 eV, which is larger than the bulk band gap of bulk CZTS (1.4–1.5 eV) [22,23]. This increase in band gap due to the small size of the particle is obviously caused by the quantum confinement effect [24].

The formation mechanism of CZTS quantum dots involves three steps. In the first step, Cu^{2+}, Zn^{2+}, and Sn^{4+} coordinated with thiourea molecules to form Cu–Thiourea, Zn–Thiourea, and Sn–Thiourea complexes [30]. Among these three complexes, The Cu–Thiourea complexes first undergo decomposition to form $Cu_{2-x}S$ nucleus. In the second step the Zn–Thiourea and Sn–Thiourea complexes undergo decomposition to form ZnS and SnS. In the third and final stage the active $Cu_{2-x}S$ reacts with ZnS and SnS to form CZTS as a stable product. At this process, the binary copper sulfide serves as the starting point for the nucleation and growth of CZTS. Meanwhile, the copper sulfide nucleus gradually disappear and transform into CZTS grains and aggregate together to form a spherical structure and it conserves the lowest surface energy. This process is agreement with previous reports [31,32].

In conclusion, high yield CZTS quantum dots have been synthesized by using simple precursors by co-precipitation technique. X-ray diffraction pattern, X-ray photoelectron spectra (XPS) and Raman spectra revealed the formation of tetragonal type pure kesterite structure CZTS nanoparticles. STEM analysis indicates the presence and uniform distribution of Cu, Zn, Sn and, S. The optical band gap shifted to the higher energy side 1.58 eV shows the presence of quantum confinement effect.

Acknowledgements

The authors thank the Department of Physics and Technology, University of Bergen, Bergen, Norway for providing necessary support to carry out this research work at Norway. Our thanks to Ing. Alvaro Angeles of LANE, Cinvestav, Mexico for the HRTEM analysis.

References

[1] P. jackson, D. Hariskos, E. Lotter, S. paetel, R. Wuerz, R. menner, et al, New world record efficiency for Cu(In,Ga)Se_2 thin-film solar cells beyond 20%, Prog. Photovoltaics Res. Appl. 19 (2011) 894–897.

[2] Ming Wei, Qingyang Du, Dacheng Wang, Weifeng Liu, Guoshun Jiang, Changfei Zhu, Synthesis of spindle-like kesterite Cu_2ZnSnS_4 nanoparticles using thiorea as sulfur source, Mater. Lett. 79 (2012) 177–179.

[3] Kunihiko Tanaka, Masatoshi Oonuki, Noriko Moritake, Hisao Uchiki, Cu_2ZnSnS_4 thin film solar cells prepared by non-vacuum processing, Sol. Energy Mater. Sol. Cells 93 (2009) 583–587.
[4] L.M. Peter, Towards sustainable photovoltaics: the search for new materials, Philos. Trans. Ser. A: Math. Phys. Eng. Sci. 369 (2011) 1840–1856.
[5] T. Todorov, O. Gunawan, S.J. Chey, T.G. de Monsabert, A. Prabhakar, D.B. Mitzi, Progress towards marketable earth-abundant chalcogenide solar cells, Thin Solid Films 519 (2011) 7378–7381.
[6] B.K. Meyer, P.J. Klar, Sustainability and renewable energies – a critical look at photovoltaics, Phys. Status Solidi 5 (2011) 318–323.
[7] C.B. Murray, D.J. Norris, M.G. Bawendi, Synthesis and characterization of nearly monodisperse CdE (E = sulfur, selenium, tellurium) semiconductor nanocrystallites, J. Am. Chem. Soc. 115 (1993) 8706–8715.
[8] A.M. Smith, S. Nie, Semiconductor nanocrystals: structure, properties and band gap engineering, Acc. Chem. Res. 16 (2010) 190–200.
[9] A.J. Nozik, M.C. Beard, J.M. Luther, M. Law, R. Ellingson, J. Jhonson, Semiconductor quantum dots and quantum dot arrays and applications of multiple excition generation to third generation photovoltaic solar cells, Chem. Rev. 110 (2010) 6873–6890.
[10] V. IKlimov, Spectral and dynamical properties of multiexcitions in semiconductor nanocrystals, Annu. Rev. Phys. Chem. 58 (2007) 635–673.
[11] O.E. Semonin, J.M. Luther, S. Choi, H.Y. Chen, J. Gao, A.J. Nozik, M.C. Beard, Peak external photocurrent quantum efficiency exceeding 100% via MEG in a quantum dot solar cell, Science 334 (2011) 1530–1533.
[12] W. Shockley, H.J. Queisser, Detailed balance limit of efficiency of Pn junction solar cells, J. Appl. Phys. 32 (1961) 510–519.
[13] M. Cao, Y. Shen, A mild solvothermal route to kesterite quaternary Cu_2ZnSnS_4nanoparticles, J. Cryst. Growth 318 (1) (2011) 1117–1120.
[14] Q. Guo, H.W. Hillhouse, R. Agrawal, Synthesis of Cu_2ZnSnS_4 nano crystal ink and its use for solar cells, J. Am. Chem. Soc. 131 (33) (2009) 11672–11673.
[15] T.K. Todorov, K.B. Reuter, D.B. Mitzi, High-efficiency solar cell with earth-abundant liquid-processed absorber, Adv. Mater. 22 (20) (2010) E156–E159.
[16] R. Sarvana Kumar, B.D. Ryu, S. Chandramohan, J.K. Seol, S.K. Lee, C-.H. Hong, Rapid synthesis of sphere-like Cu_2ZnSnS_4 microparticles by microwave irradiation, Mater. Lett. 86 (2012) 174–177.
[17] D.B. Mitzi, O. Gunawan, T.K. Todorov, K. Wang, S. Guha, The path towards a high-performance solution-processed kesterite solar cell, Sol. Energy Mater. Sol. Cells 95 (6) (2011) 1421–1436.
[18] Christopher A. Cattley, Cheng Cheng, Simon M. Fairclough, Laura M. Droessler, Neil P. Young, Jamie H. Warner, Jason M. Smith, Hazel E. Assender, Andrew A.R. Watt, Low temperature phase selective synthesis of Cu_2ZnSnS_4 quantum dots, Chem. Commun. 49 (2013) 3745–3747.
[19] Huanping Zhou, Wan-Ching Hsu, Hsin-Sheng Duan, Brion Bob, Wenbing Yang, Tze-Bin Song, Chia-Jung Hsu, Yang Yang, CZTS nanocrystals: a promising approach for next generation thin film photovoltaics, Energy Environ. Sci. 6 (2013) 2822–2838.
[20] JCPDS, card no. 26-0575.
[21] Kuo-Chin Wang, Peter Chen, Chuan-Ming Tseng, Facile one-pot synthesis of Cu_2ZnSnS_4 quaternary nanoparticles with microwave-assisted method, CrystEngComm 15 (2013) 9863–9868.
[22] A. Singh, H. Geaney, F. Laffir, K.M. Ryan, Colloidal synthesis of wurtzite Cu_2ZnSnS_4 nanorods and their perpendicular assembly, J. Am. Chem. Soc. 134 (2012) 2910–2913.
[23] H. Yang, L.A. Jauregui, G. Zhang, Y.P. Chen, Y. Wu, Nontoxic and abundant copper zinc tin sulfide nanocrystals for potential high-temperature thermoelectric energy harvesting, Nano Lett. 12 (2012) 540–545.
[24] Narayanasamy Sabari Arul, Dong Yeol Yun, Dea Uk Lee, Tae Whan Kim, Strong quantum confinement effects in kesterite Cu_2ZnSnS_4 nanospheres for organic optoelectronic cells, Nanoscale 5 (2013) 11940–11943.
[25] W.C. Liu, B.L. Guo, X.S. Wu, F.M. Zhang, C.L. Mak, K.H. Wong, Facile hydrothermal synthesis of hydrotropic Cu_2ZnSnS_4 nanocrystal quantum dots: band-gap engineering and phonon confinement effect, J. Mater. Chem. A 1 (2013) 3182–3186.
[26] Shulin Ji, Tongfei Shi, Xiaodong Qiu, Jian Zhang, Guoping Xu, Chao Chen, Zheng Jiang, Changhui Ye, A route to phase controllable $Cu_2ZnSn(S_{1-x}Se_x)_4$ nanocrystals with tunable energy bands, Sci. Rep. 3 (2013) 2733.
[27] G. Rajesh, N. Muthukumarasamy, E.P. Subramaniam, S. Agilan, Dhayalan Velauthapillai, Synthesis of Cu_2ZnSnS_4 thin films by dip-coating method without sulphurization, J. Sol–Gel Sci. Technol. 66 (2013) 288.
[28] Q.J. Guo, H.W. Hillhouse, R. Agrawal, Synthesis of Cu_2ZnSnS_4 nano crystal ink and its use for solar cells, J. Am. Chem. Soc. 131 (2009) 11672–11673.
[29] P.A. Fernandes, P.M.P. Saloméa, A.F. da Cunhaa, Study of polycrystalline Cu_2ZnSnS_4 films by Raman scattering, J. Alloys Compd. 509 (2011) 7600–7606.
[30] D. Chen, K.B. Tang, G.Z. Shen, J. Sheng, Z. Fang, X.M. Liu, H.G. Zheng, Y.T. Qian, Microwave-assisted synthesis of metal sulfides in ethylene glycol, Mater. Chem. Phys. 82 (2003) 206–209.
[31] L.S. Zhong, J.S. Hu, H.P. Liang, A.M. Cao, W.G. Song, L.J. Wan, Self-assembled 3D flowerlike iron oxide nanostructures and their application in water treatment, Adv. Mater. 18 (2006) 2426–2431.
[32] M.H. Tang, Q.W. Tian, X.H. Hu, Y.L. Peng, Y.F. Xue, Z.G. Chen, J.M. Yang, X.F. Xu, J.Q. Hu, *In situ* preparation of $CuInS_2$ films on a flexible copper foil and their application in thin film solar cells, CrystEngComm 14 (2012) 1825–1832.
[33] C. Persson, Electronic and optical properties of Cu_2ZnSnS_4 and $Cu_2ZnSnSe_4$, J. Appl. Phys. 107 (2010) 053710-1–053710-8.
[34] J. Paier, R. Asahi, A. Nagoya, G. Kresse, Cu_2ZnSnS_4 as a potential photovoltaic material: a hybrid Hartree-Fock density functional theory study, Phys. Rev. B 79 (2009) 115126-1–115126-8.